72nd International Astronautical Congress (IAC), Dubai, United Arab Emirates, 25-29 October 2021.

IAC-21,A5,3-B3.6,5

Terrain-Aware Communication Coverage Prediction for Cooperative Networked Robots in Unstructured Environments

Emanuel Staudinger[1], Riccardo Giubilato[2], Martin J. Schuster[2], Robert Pöhlmann[1], Siwei Zhang[1], Andreas Dömel[2], Armin Wedler[2], and Armin Dammann[1]
[1]Department of Communication Systems, Institute of Communications and Navigation, German Aerospace Center (DLR) e.V., Oberpfaffenhofen, Germany, firstname.lastname@dlr.de
[2]Department of Perception and Cognition, Institute of Robotics and Mechatronics, German Aerospace Center (DLR) e.V., Oberpfaffenhofen, Germany

Networked robots will play an important role in lunar exploration. Communication is key to enable cooperation among robots for information sharing, and to remotely control robots with lower degree of autonomy from a lander or habitat. Operators and scientists must be able to make sound decisions on communication availability before or during sending robots to regions of interest for exploration. In this work we have a closer look at the communication coverage prediction for lunar exploration. We present an interdisciplinary and modular framework, which exploits terrain information to predict the data rate for exploring robots. Additionally, we create intuitively usable coverage maps for operators and scientists, and show how connectivity can be improved in unstructured environments by using a relay rover. This paper provides an overview of this framework, details on individual framework components, and simulation results for two exemplary exploration scenarios.

Keywords: Wireless Communications, Robotic Exploration, Moon, Semantic Annotation, Path Loss, Cooperation

I. Introduction

The moon regained significant interest for exploration over the past years [1]. The HERACLES program from the European Space Agency (ESA) or the ARTEMIS program from the National Aeronautics and Space Administration (NASA) foresee multiple robots and humans jointly exploring the lunar surface in the vicinity of a lander or a habitat [2], [3]. Robots, deployed sensors, and interacting humans can be seen as one cooperative network. In particular for robots with varying degrees of autonomy, a communication link to the lander or habitat is required [4]. For example, processing tasks of the robots demanding high computational power can be offloaded to the lander. Scientific data of multi-spectral cameras must be communicated back to scientists and operators to determine next execution steps. Moreover, operators in the habitat want to remotely operate robots in the exploration area, e.g., for difficult manipulation tasks not yet achievable with currently available autonomous space robotics technology. Communication is key for such networks and all before mentioned aspects [4], [5].

Let us have a look at an exemplary exploration scenario on the lunar surface in Fig. 1. A science rover shall visit multiple regions of interest, with the trajectory starting and ending at the lander. Regions of interest include small craters, rocky outcrops, and rock structures in plain field. For a successful mission one might ask if the science rover can operate in the regions of interest? Is communication available to communicate data from scientific instruments and perform remotely controlled manipulation, and could we predict the communication link quality to support operators and scientists for sound decision making? In this work, we have a particular look at the coverage prediction for networked robots including terrain information, and providing intuitively usable coverage information to operators and scientists. We propose an interdisciplinary modular framework to this goal, provide details and simulation results.

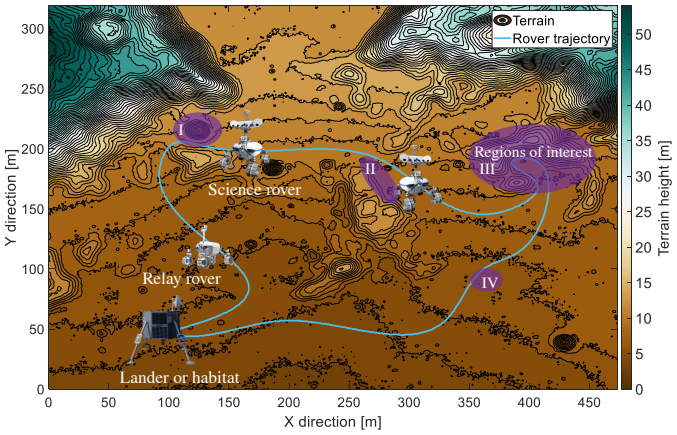

Fig. 1: Exploration scenario on lunar terrain. A science rover must visit multiple regions of interest along a traversable trajectory. A dedicated relay rover can support for communication from the science rover to the lander or habitat to enable heavy processing within the lander or closed-loop remote control for manipulation.

This paper is organized as follows: Sec. II introduces our framework and provides an overview. The generation of a 2.5 D map and semantic annotation are described in Sec. III,

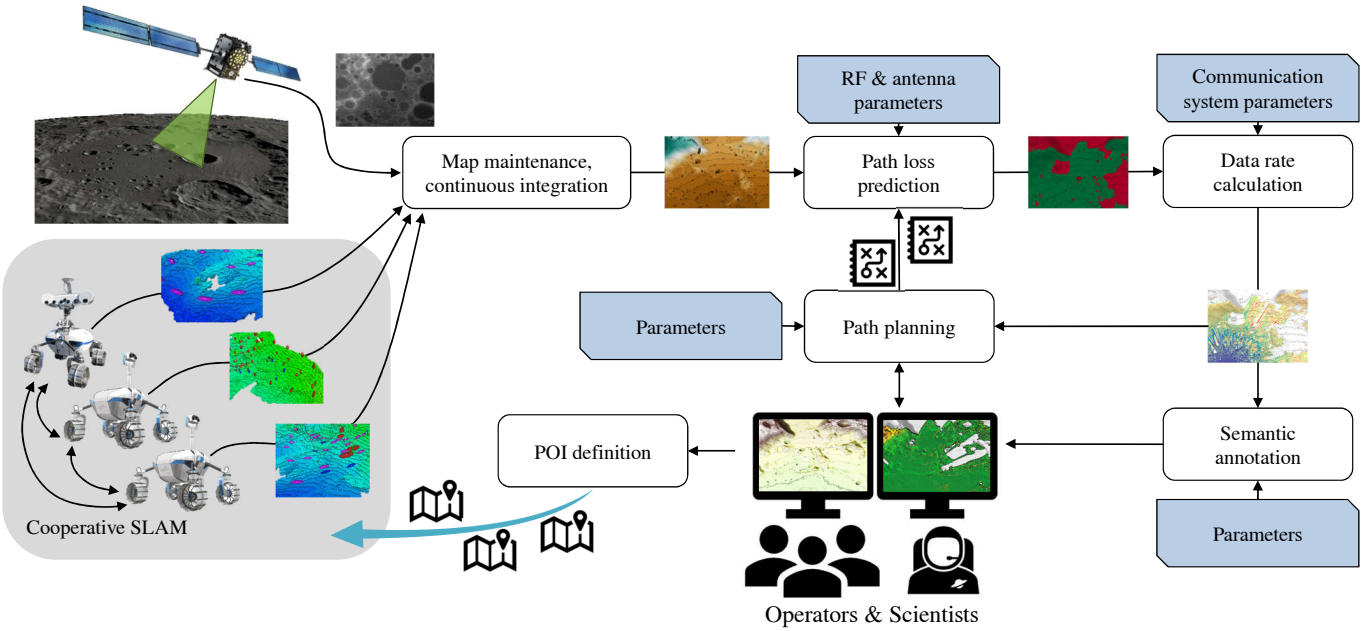

Fig. 2: Overview of the interdisciplinary framework for wireless coverage prediction. 2.5 D maps jointly created by satellite(s) and robots are used to predict the radio signal's path loss and detailed data rate map. The semantic annotation creates intuitively usable maps for operators and scientists to define the next point of interest (POI) or evaluate connectivity along robot trajectories.

followed by a more detailed description of the path loss prediction and data rate calculation in Sec. IV. Simulation results from our framework for the static case, as well as for a relaying example, can be found in Sec. V and Sec. VI respectively, followed by a short discussion and outlook in Sec. VII.

II. Coverage Prediction Framework

An overview of our coverage prediction framework is shown in Fig. 2. We describe individual components on a higher level next, and provide details in subsequent sections. The framework is realized in the software Matlab and Robot Operating System (ROS) and interdisciplinary in the sense that the robotics/computer science domain and the telecommunications/electrical engineering domain join forces to create such a framework. It comprises modular and parameterizable components to enable, e.g., parameters sweeps for design exploration.

The first step for coverage prediction is the generation of a 2.5 D elevation map. Global terrain information as digital elevation map (DEM) is commonly available from satellites with coarse resolution, for example elevation maps produced by the lunar reconnaissance orbiter. On the surface, multiple robots explore an area of interest and use visual navigation to simultaneously map the environment and locate themselves within it. By sharing observations of the environment and through the measurement of each others' relative positions, the robotic network can cooperatively create a high resolution map of the surface in the form of a 3D point cloud. The map maintenance component in the framework combines maps from various sources and modalities and creates a 2.5 D elevation map with continuous updates.

The path loss prediction component makes use of the 2.5 D map to determine the path loss of the radio signal, from which a link budget for data rate calculation can be determined. The data rate calculation component provides a very detailed data rate map showing, e.g., the resulting data rate and connectivity for an exploration area where a lander serves as communication base station. In most cases, the data rate map is too detailed for an operator or scientist for intuitive usage.

Hence, a semantic annotation component simplifies the created maps, such that operators and scientists get intuitively usable information: for example, to quickly identify if an exploration area or POI is covered by communication or not. In a particular exploration scenario, a robot can autonomously navigate to a POI without communication, yet scientists wish to examine multi-spectral images from the robot and conduct remote manipulation for which communication is mandatory.

The operators can use a path planning component to determine connectivity of the robots along already planned or future trajectories. Additionally, a communication relay rover can be integrated to enhance communication for the main science rover, and to obtain optimal positions for the communication relay rover.

III. Map Maintenance and Semantic Annotation

As introduced in Sec. II, the presented communication coverage prediction framework relies on two main components: one creates and handles maps of the environment, and the other uses the provided knowledge of the terrain elevation to infer the quality of the communication. In this section, details are given about the first component, where an estimation of the geometry of the environment is produced using all available inputs from either satellites or robotic agents.

A. Map Building and Maintenance

Knowledge of the geometry of the terrain plays a critical role in the processing pipeline described in this work. In the context of teams of mobile robots operating in unstructured and partially unknown environments, the tasks of mapping and localization are solved simultaneously by performing multi-agent SLAM (Simultaneous Localization and Mapping). At the DLR Institute of Robotics and Mechatronics, a SLAM system has been developed targeted to a group of heterogeneous robots [6], [7] that includes, but is not limited to, two ground rovers, the LRU (Lightweight Rover Unit) [8], and a flying robot, ARDEA [9]. Both are equipped with a stereo camera and an inertial measurement unit (IMU) to compute odometry and to build gravity-aligned submaps, which are local representations of the environment in the form of point clouds. A local reference frame defines the position of each submap with respect to the origin of the mapping session and constitute nodes in a graph that is continuously optimized by the SLAM algorithm. The point cloud in each submap is used to compute 3D feature descriptors that unambiguously identify details in local structures and that can be used to detect matching structures in other submaps. This way, by means of submap matching, additional constraints are added to the graph that correct the local origins of submaps from odometry errors, improving the consistency of the global map. In addition, all the robots belonging to the team can compute their respective position one to the other by observing visual markers rigidly mounted on the robot's body. Graph corrections follow each submap match or robot detection and therefore act as a continuous maintenance routine of the global map. As the global map is referred to the position of the lander, whose position is known in a specific geographic reference frame, the elevation data from satellite DEMs can be fused with the map built by the team of robot in a Bayesian fashion. This allows to obtain maps of a larger coverage and different levels of detail on the elevation.

B. Semantic Annotation

The global 2.5D map resulting after the steps in Sec. III-A is published in the ROS network using the GridMap library [10] and used to predict path loss and data rate as explained in Section IV. Fig. 3 graphically highlights the interactions between each component of the pipeline related to the task of producing semantically annotated maps for the operators. Elevation, data rate and line-of-sight (LOS) predictions are handled as images. The elevation image is used to compute a grayscale representation of the terrain through the process of hill shading, where a simulated light source casts shadows on the terrain highlighting the shape of hills and valleys. The values of the predicted data rate are used to produce a color image that categorizes values in ranges that are configurable from the operators and that are meaningful to assess the quality of the communication (e.g. $\{5, 10, 20, 50, 75, 100\}$ Mbps). The line of sight prediction is used to identify zones in the data rate image where communication is not possible. Finally, all images are combined to produce visual maps that highlight both, the structure of the environment, as well as the quality of the communication. Fig. 6 shows examples of resulting semantically annotated maps.

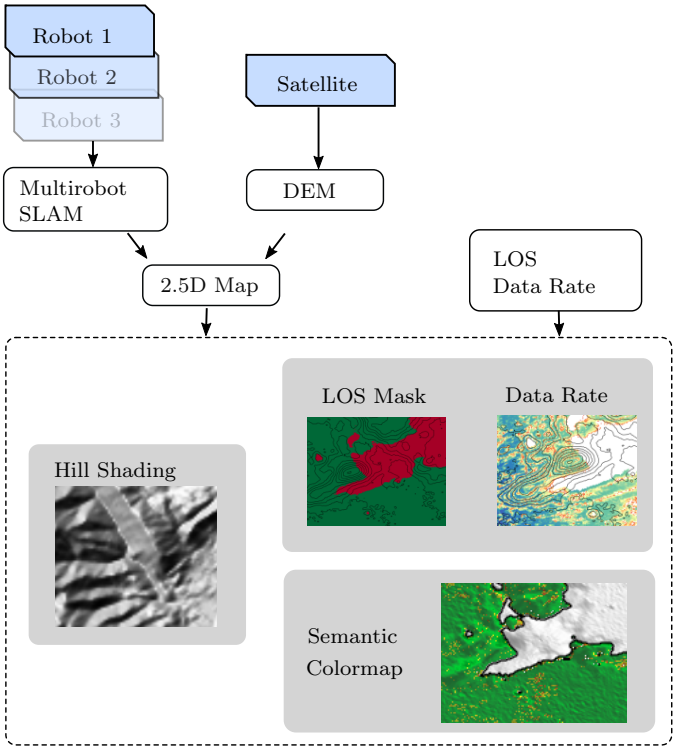

Fig. 3: Workflow of the semantic annotation pipeline as a result of the interaction between the online building and maintenance of a multi-agent map (Sec. III) and communication coverage prediction (Sec. IV).

IV. Path Loss and Data Rate Prediction

Prediction of the data rate at a certain location comprises two buildings blocks: predicting the path loss based on a radio propagation model and terrain data, and calculating the expected data rate with a communication system model.

A. Radio Propagation Modeling

Various radio propagation models from the field of mobile radio communications exist, which can be applied to our framework [11]. In general, radio propagation models to predict the path loss at a specific location and time consist of deterministic and stochastic components. In this work, we focus on deterministic large scale fading effects and deterministic components only. We take the LOS component and the ground reflection component into account, which is commonly referred to as 2-path ground reflection model [11]. We assume vertical polarization and discard diffraction effects. For radio frequency (RF) signals above 1 GHz, diffraction effects can be neglected in a purely hilly terrain environment, where no infrastructure such as buildings is present.

The process to predict the path loss for a specific transmitter and receiver position within the terrain, given the terrain as grid based 2.5D map, is as follows:

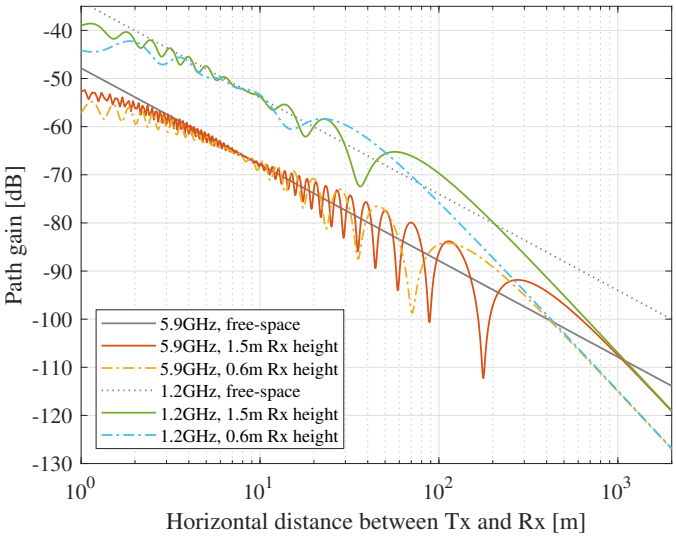

Fig. 4: 2-path model path gain for two carrier frequencies and two receiver antenna heights. The free-space path gain is provided as reference. The radio wave reflected from the ground results in a spatial interference pattern, and beyond a breakpoint distance, the path gain decays twice as fast compared to free-space.

1) Determine if LOS is blocked. If it is blocked we can skip all further calculations, as no connectivity is possible.
2) Extract tiles of the map between Tx and Rx position based on Bresenham's algorithm and determine LOS blockage for each terrain point between the point on the ground and Tx/Rx antennas. This pre-selects ground reflection candidates which have possible connectivity to Tx and Rx.
3) Determine incident and emergent angles for pre-selected ground reflection candidates and determine the most valid ground reflection point.
4) Calculate reflection coefficient and additional path delay for ground reflection signal, and determine resulting path loss. We also take incident and emergent angles at Tx and Rx antenna for both, the LOS component and ground reflection component into account to determine angle-specific antenna gains for given antenna patterns.

Compared to [12], [13] we take the complex permittivity of the ground into account, and do not fix the reflection coefficient to a value of -1. We also do not make use of the Fresnel zone concept, as it actually applies to highly directed antennas, and is not the optimal model for the antennas assumed in this work.

Fig. 4 shows examples of resulting path gains – the negative path loss in logarithmic domain – for two different carrier frequencies and receiver antenna heights over flat terrain. The transmitter antenna is at a height of $3\,\mathrm{m}$, and we assume omni-directional vertically polarized antennas. Complex permittivity of the ground is $\epsilon = 3.5 - j0.25$ for both carrier frequencies, which relates to a very dry, sandy soil [14]. The reflected radio signal from the ground creates constructive or destructive interference on the LOS signal component, depending on the phase difference between both signals. As a result, we can clearly see this interference effect in Fig. 4. At certain Tx-Rx distances, we get destructive interference and the path gain is significantly lower compared to the free space model. Hence, communication link quality can be severely degraded. The choice of receiver antenna height has a major impact on the spatial interference pattern. As a consequence, the receiver antenna height can be a design choice during system design. At larger distances we can see that the path gain decays twice as fast compared to the free space model, and the path gain curves for a fixed receiver antenna height converge regardless of the carrier frequency.

TABLE I: Parameters of Communication System Model

Parameter	Value
Carrier frequency	$5.9\,\mathrm{GHz}$
Transmit power	$100\,\mathrm{mW}$
Signal bandwidth	$40\,\mathrm{MHz}$
Receiver temperature	$293\,\mathrm{K}$
Receiver noise figure	$7\,\mathrm{dB}$
SNR detection threshold	$1\,\mathrm{dB}$
Coding rate	$1/3$

The complex permittivity of the ground plays in general an important role in the propagation model as it additionally models ground conductivity [14]. To gain insight how sensitive our propagation model w.r.t. those parameter changes is, we evaluated the path gain for a relative permittivity or the conductivity increased by a factor of ten. We can conclude, that the path gain does change, in particular the spatial positions of the deep fades and their values, yet the overall spatial interference shape remain similar. Other effects, such as the accuracy of the terrain map or antenna height above ground, contribute significantly more to the propagation model.

B. Communication System Model

In this work, we model the communication system based on calculated link budgets and the Shannon formula. We assume an orthogonal frequency-division multiplexing (OFDM) modulation based transceiver with bandwidths commonly used in state of the art wireless communication standards such as 802.11p, 3GPP-LTE, or 5G. In a first step we calculate the link budget based on an assumed transmit power at the RF port of the transmit antenna and the path gain from Sec. IV-A. We also take the receiver noise temperature, noise bandwidth, and an additional noise figure into account. Every receiver has a detection threshold, above which it can successfully detect received signal frames, and perform channel estimation for equalization. For our OFDM system model, we use a signal to noise ratio (SNR) threshold of $1\,\mathrm{dB}$. If the SNR is below this threshold, we cannot detect signal frames and, thus, no connectivity between transmitter and receiver is possible.

In a second step, we use the Shannon formula with the modified SNR value from the first step, and the transmission bandwidth to calculate an expected data rate. A practical communication system for a space application might not have adaptive coding and modulation (ACM) schemes implemented. Hence, we assume a conservative implementation with a fixed coding rate of $1/3$. Tab. I summarizes the

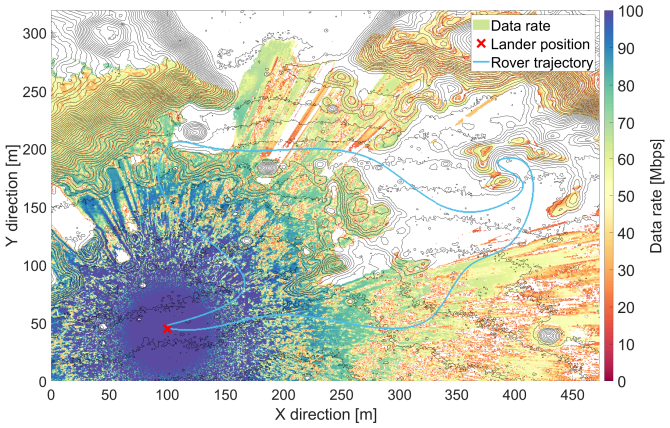

Fig. 5: Detailed data rate map showing the wireless coverage of the lander. The color coding is saturated at 100 Mbps. No connectivity is possible in white areas.

communication system model parameters applied in this work. Those values can be chosen flexibly to tailor the framework to a specific application.

V. Results - Static Coverage Maps

In the static coverage maps case we predict the wireless coverage from the lander point of view, with the lander as transmitter and a rover or sensor payload box as receiver. We use a dipole antenna with 10 dBi antenna gain at the lander, and a zero-gain omnidirectional antenna for the rover. One can afford to use a larger physical antenna on the lander w.r.t. the carrier wavelength, compared to a light-weight rover. The lander antenna height is 3 m and we apply the communication system model parameters from Tab. I.

Fig. 5 shows the resulting detailed data rate coverage map for a rover with a receiver antenna height of 1 m. We can clearly see the shadowed areas in white color, where the LOS component is blocked due to hills or where the rover is inside a crater and the crater rim is blocking the radio signal. The predicted data rate is not monotonously decreasing over distance in flat regions, because the ground reflection component interferes with the LOS component, see Fig. 4 for comparison. At larger distances from the lander, the received LOS component can already be weak, so that the interfering ground reflection component leads to a loss in connectivity. We can observe that in particular in the x-direction range between 260 m and 450 m at low y-direction values.

The coverage map in Fig. 5 provides very detailed information about the expected data rate at certain locations and the expected loss of connectivity. This information is jointly processed with the 2.5D map information in the semantic annotation block to provide an intuitively understandable coverage map for an operator, see also Fig. 2 and Sec. III. Fig. 6 shows the semantically annotated maps as final product for the operator. The terrain is annotated to emphasize craters and hills through the selected color shading and contour lines, see Fig. 6a. Fig. 6b-d depict the annotated data rate jointly with the terrain profile for three different receiver antenna heights. From those annotated results we can clearly see the coverage differences w.r.t. receiver antenna height.

In addition to providing intuitively usable maps for an operator, we can extract the predicted data rate along the rover trajectory as shown in Fig. 1. The resulting data rate along the track, visiting science goals I to IV from Fig. 1, is shown in Fig. 7. For the carrier frequency of 5.9 GHz we observe two main aspects along the trajectory. Firstly, we see the loss of connectivity with a data rate of 0 Mbps for two parts of the trajectory between 270 m-320 m and 450 m-800 m. Secondly, we can see rapid variations in the data rate over the trajectory length, where the data rate drops by approximately 50 % to 75 % over few meters of distance along the trajectory. In general, we can observe that once connectivity is available, the resulting data rate is high, e.g. above 30 Mbps for the 5.9 GHz radio link and for our model parameters.

Our flexible framework enables the evaluation with different parameters for the wireless communication system. Hence, we are also interested in how the predicted data rate along the trajectory changes if we select a different carrier frequency. All parameters except the complex permittivity of the soil are equivalent to the 5.9 GHz use case. The relative permittivity is kept constant, but the conductivity has been reduced according to [14], though we did not see major differences in resulting path losses in prior simulations. The dashed line in Fig. 7 shows results for a carrier frequency of 1.2 GHz. Again, we can see two main aspects. Firstly, the loss of connectivity between 270 m-320 m and 450 m-800 m is equivalent to the 5.9 GHz use case due to the LOS blockage. Secondly, the data rate variation along the trajectory is lower: at some track positions a drop in data rate is visible, yet it is smaller compared to the 5.9 GHz use case.

Based on the results of this section we can conclude: A lower carrier frequency is beneficial to mitigate rapid data rate changes along the trajectory, at the cost of a larger physical antenna. The main source of connectivity loss is LOS blockage due to large rocks and hills. Higher antenna masts for both, the lander and the exploring robot can be used, although this might be limited due to physical structural constraints, and does not solve the problem in general, if hills or rocks are higher than expected. A possible solution is the usage of an additional robot as communication relay, which we are discussing and evaluating in the following section.

VI. Results - Dynamic Coverage Maps

In this work, we also investigate how the connectivity gaps along the trajectory of the exploring science robot can be mitigated through a second rover operating as a communication relay. The so-called relay rover uses an omnidirectional antenna at a height of 1.5 m and the same communication model parameters as the exploring robot. We assume a carrier frequency duplex, and the exploring rover always communicates with the lander over the relay rover for simplicity: no horizontal handover is performed.

Based on our framework we are now interested in optimal positions for the relay rover. Those optimal positions can then be given as navigation goal to the relay rover by an operator,

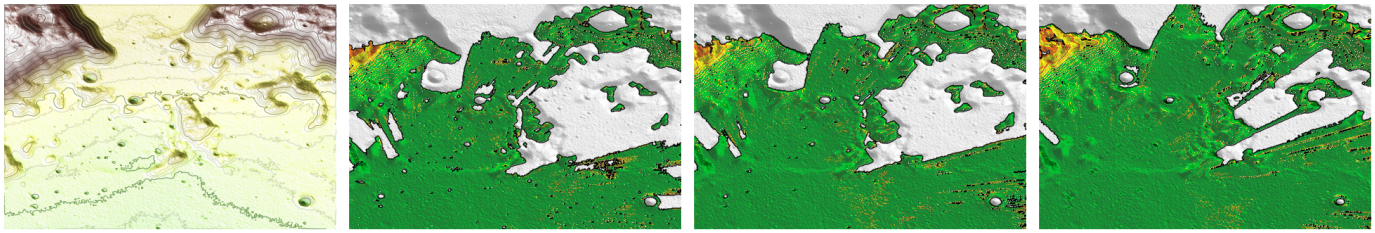

(a) Height map with contour lines. (b) 0.4 m receiver antenna height. (c) 1.0 m receiver antenna height. (d) 3.0 m receiver antenna height.

Fig. 6: Generated maps presented to the operator after semantic annotation of the height map and the predicted data rate map. The wireless coverage maps clearly show the benefit of a larger receiver antenna height. The semantic annotation enables an intuitive experience for the operator.

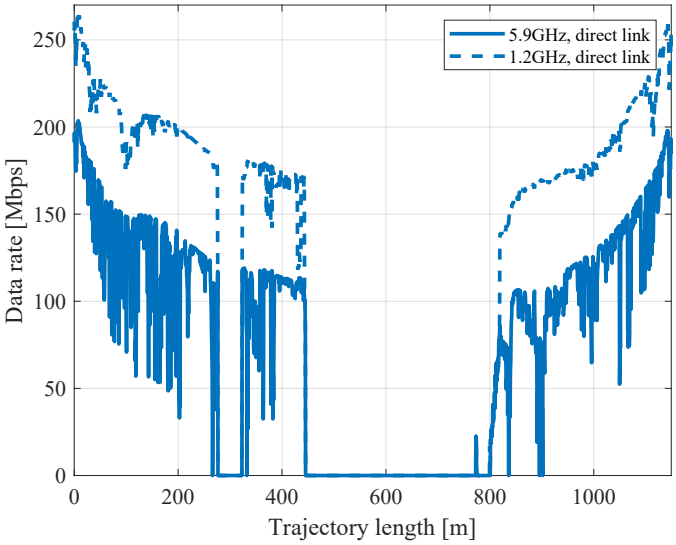

Fig. 7: Data rate along the trajectory for direction communication between the science rover and the lander for two different carrier frequencies. The lower frequency link shows smaller rapid variations compared to the higher frequency link. Two large connectivity gaps are present due to LOS blockage.

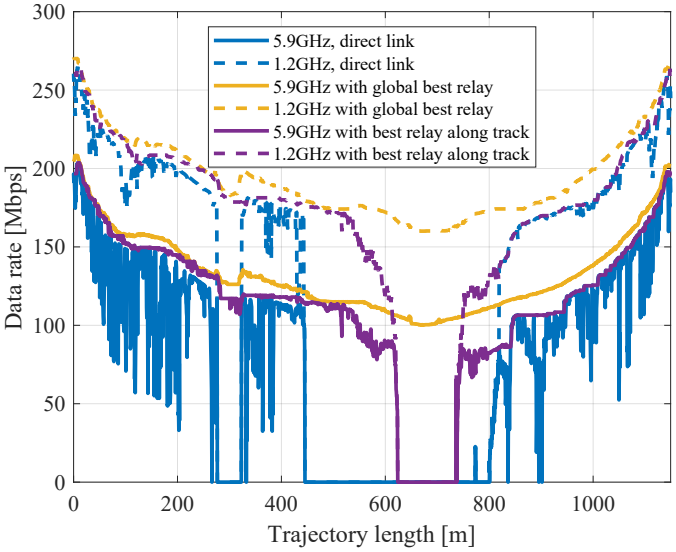

Fig. 8: Data rate along trajectory for two relaying scenarios: the global best relay position, and the relay located along the track between the lander and the science rover's position. Rapid data rate variations as well as the loss of connectivity are significantly reduced.

or serve as input for autonomous waypoint navigation and control. We have a look at two optimal position scenarios for comparison. In the first scenario we determine the globally best relay rover position in the map. Although this scenario is not practical, because the optimal relay rover position could jump within the map, we obtain an upper limit for the predicted data rate. For the second scenario we assume that the exploring science rover provides detailed environment information for visual navigation along the trajectory and communicates resulting maps to the relay rover. In such a scenario the relay rover can be a very tailored micro-rover with minimum visual navigation and processing capabilities. Optimal relay rover positions can then only be determined along the trajectory from the lander to the current position of the exploring science robot. For simulation, we divide the trajectory into 3000 locations, for which we re-compute the coverage between relay rover and the science rover positions.

Fig. 8 shows resulting data rates for the direct link (as in Fig. 7), the global best relay, and the best relay along track for 1.2 GHz and 5.9 GHz. We observe three main results:

1) The connectivity loss at trajectory length 270 m-320 m can be completely avoided. Between 450 m-800 m the connectivity loss is significantly reduced, yet due to the terrain, no link can be established between 620 m-740 m.
2) Using a relay link significantly reduces rapid data rate variations along the trajectory, particularly for the 5.9 GHz radio link.
3) The global best relay data rate is always greater than 0 Mbps: connectivity is in principle achievable throughout the entire trajectory.

Additionally, we should note, that the data rate for the best relay along track scenario can potentially be below the direct link scenario. This is due to the assumption that the science rover does not make a horizontal handover and always uses the communication relay. Hence, the results of the best relay along track cannot strictly be seen as an overbound of the direct link result.

VII. Conclusion and Outlook

In this work we presented an interdisciplinary framework to predict wireless coverage over unstructured terrain for cooperative networked robots. Resulting coverage maps are generated for intuitive usage by operators and scientists determining POIs for robots, or planning robot trajectories. From our simulations we can conclude that LOS blockage due to large hills and rock structures are the main cause of connectivity loss and antenna height is crucial. Once LOS is available the data rate is high enough for most use cases. Only at larger distances where the LOS signal is very weak, we identify a loss of connectivity due to radio wave interference from the ground reflection. Directed antennas at the lander can be used to mitigate the ground reflection effect. In the relaying scenario we identify the need for more relay rovers to achieve connectivity for the science rover throughout the trajectory.

As a next step we want to put this framework to a test. We are currently finalizing integration of this framework for a real demonstration in the Autonomous Robotic Networks to Help Modern Societies (ARCHES) project taking place on Mount Etna, Sicily, Italy, planned for summer 2022. The applied radio propagation model assumes two deterministic components only. The stochastic contribution of a radio propagation model could potentially be used to derive uncertainty of the predicted data rate. Additionally, we will use this framework in the context of our swarm-navigation system to predict coverage among dozens of robotic agents [15].

Acknowledgment

Part of the presented research has been supported by the Helmholtz Association project ARCHES (contract number ZT-0033) and the German Aerospace Center (DLR) project Planetary Exploration.

References

[1] "Global exploration roadmap, supplement august 2020, lunar surface exploration scenario update," International Space Exploration Coordination Group, Tech. Rep. NP-2020-07-2888-HQ, 2020.

[2] H. Hiesinger, M. Landgraf, W. Carey, Y. Karouji, T. Haltigin, G. Osinski, U. Mall, K. Hashizume, Heracles Science Working Group, and Heracles International Science Definition Team, "HERACLES: An ESA-JAXA-CSA Joint Study on Returning to the Moon," in *Lunar and Planetary Science Conference*, ser. Lunar and Planetary Science Conference, Mar. 2019, p. 1327.

[3] "Nasa's lunar exploration program overview," International Space Exploration Coordination Group, Tech. Rep. NP-2020-05-2853-HQ, Sep. 2020.

[4] S. Zhang, E. Staudinger, R. Pöhlmann, and A. Dammann, "Cooperative communication, localization, sensing and control for autonomous robotic networks," in *IEEE International Conference on Autonomous Systems (IEEE ICAS 2021)*, August 2021. [Online]. Available: https://elib.dlr.de/142695/

[5] E. Staudinger, S. Zhang, R. Poehlmann, and A. Dammann, "The role of time in a robotic swarm: A joint view on communications, localization, and sensing," *IEEE Commun. Mag.*, vol. 59, no. 2, pp. 98–104, 2021.

[6] M. J. Schuster *et al.*, "The ARCHES Space-Analogue Demonstration Mission: Towards Heterogeneous Teams of Autonomous Robots for Collaborative Scientific Sampling in Planetary Exploration," *IEEE Robotics and Automation Letters (RA-L)*, vol. 5, no. 4, pp. 5315–5322, Oct 2020.

[7] M. J. Schuster, K. Schmid, C. Brand, and M. Beetz, "Distributed stereo vision-based 6d localization and mapping for multi-robot teams," *Journal of Field Robotics (JFR)*, 2018. [Online]. Available: https://onlinelibrary.wiley.com/doi/abs/10.1002/rob.21812

[8] M. J. Schuster *et al.*, "Towards Autonomous Planetary Exploration: The Lightweight Rover Unit (LRU), its Success in the SpaceBotCamp Challenge, and Beyond," *Journal of Intelligent & Robotic Systems (JINT)*, Nov. 2017. [Online]. Available: https://doi.org/10.1007/s10846-017-0680-9

[9] P. Lutz, M. G. Müller, M. Maier, S. Stoneman, T. Tomić, I. von Bargen, M. J. Schuster, F. Steidle, A. Wedler, W. Stürzl *et al.*, "Ardea—an mav with skills for future planetary missions," *Journal of Field Robotics*, vol. 37, no. 4, pp. 515–551, 2020.

[10] P. Fankhauser and M. Hutter, "A universal grid map library: Implementation and use case for rough terrain navigation," in *Robot Operating System (ROS)*. Springer, 2016, pp. 99–120.

[11] T. S. Rappaport, *Wireless communications - principles and practice.* Prentice Hall, 1996.

[12] S. Santra, L. B. Paet, E. Staudinger, M. Laine, and K. Yoshida, "Experimental validation of deterministic radio propagation model developed for communication-aware path planning," in *2021 IEEE 17th International Conference on Automation Science and Engineering (CASE)*. IEEE, 2021, pp. 1–6.

[13] S. Santra, L. B. Paet, E. Staudinger, and K. Yoshida, "Radio propagation modelling for coordination of lunar micro-rovers," in *International Symposium on Artificial Intelligence, Robotics and Automation in Space (i-SAIRAS)*. Lunar and Planetary Institute, Universities Space Research Association, Oct. 2020, pp. 1–8.

[14] "Electrical characteristics of the surface of the earth," International Telecommunication Union (ITU-R), Tech. Rep. Recommendation ITU-R P.527-4, Jun. 2017.

[15] S. Zhang, R. Pöhlmann, E. Staudinger, and A. Dammann, "Assembling a swarm navigation system: Communication, localization, sensing and control," in *2021 IEEE 18th Annual Consumer Communications Networking Conference (CCNC)*, 2021, pp. 1–9.